Measurement of the neutrons emitted in the proton-induced fission of ^{209}Bi and ^{238}U at 475 MeV

Z. Fraenkel, A. Breskin, R. Chechik, and S. Wald
Nuclear Physics Department, Weizmann Institute of Science, Rehovot 76100, Israel

R. Abegg, H. W. Fielding, P. Kitching, S. T. Lam, G. C. Neilson, W. C. Olsen, and J. Uegaki
Physics Department, University of Alberta, Edmonton, Alberta, Canada T6G 2J1
(Received 26 June 1989; revised manuscript received 15 November 1989)

We have measured the number of prefission and postfission neutrons emitted in the fission of ^{209}Bi and ^{238}U targets bombarded with 475 MeV protons as a function of the total kinetic energy of the two fission fragments, the fission fragment mass, and the recoil velocity of the excited nucleus prior to fission. The average number of prefission neutrons is approximately equal to the average number of postfission neutrons for both targets and the total number equals ~ 17. The number of prefission neutrons increases with increasing recoil velocity and their average number is substantially larger than that predicted by the Bohr-Wheeler theory.

I. INTRODUCTION

The dependence of the fission probability of a highly excited heavy nucleus on the excitation energy has long been an unsolved problem. It has been known for many years that statistical model calculations, which include fission as one of the deexcitation channels and make use of the original Bohr-Wheeler formulation[1] for the fission width, increasingly overestimate the fission probability as the excitation energy is raised. This discrepancy has generally been ascribed to the effect of nuclear dissipation which reduces the fission width, as was first shown by Kramers.[2] In a more detailed investigation Grangé *et al.*[3,4] showed that nuclear dissipation affects the fission process in three significant ways: (1) As pointed out by Kramers, fission is a quasistationary diffusion process and the strength of the coupling between the fission variable and the rest of the system is affected by the friction constant β. (2) Additional time is required by the quasistationary probability flow over the barrier. (3) Finally, as also shown by Hofmann and Nix,[5] a finite time is needed for the system to descend from the saddle point to the scission point, this time also being affected by nuclear dissipation or friction. Neutron evaporation, which is the main competing process, is not affected by nuclear dissipation, and as a result the ratio of fission width to neutron emission width is substantially lower than predicted by the Bohr-Wheeler theory, particularly at high excitation energies.

Hassani and Grangé[6] have pointed out that the number of neutrons emitted prior to fission is sensitively dependent on the effect of nuclear dissipation. Grangé *et al.*[4] and Gavron *et al.*[7] have used the number of prefission neutrons emitted in the reaction ^{16}O+^{142}Nd to estimate the size of the nuclear dissipation coefficient. Other measurements of the number of prefission and postfission neutrons have recently been performed.[8–16] However, these measurements were done for heavy-ion reactions that, in addition to a high excitation energy, also have a very high angular momentum.

It is of obvious interest to try to separate the effects of angular momentum from those of the excitation energy. This can be done by exciting the fissioning system by bombardment with high-energy protons or other light ions. Such reactions result in a highly excited nucleus with relatively little angular momentum. The disadvantage of this mode of excitation is that high-energy (>100 MeV) proton-nucleus reactions do not generally result in a compound system with a unique excitation energy. Instead the reaction consists of a fast intranuclear cascade (INC) which results in a distribution of nuclei with varying amounts of excitation energy. These excited nuclei deexcite later through particle evaporation and (for heavy nuclei) fission.

In this work we report on a study of the neutron emission in the fission of ^{209}Bi and ^{238}U targets bombarded with 475-MeV protons at the TRIUMF accelerator. Neutron energies were measured as a function of the total kinetic energy (TKE) of the fragments, the fragment mass, the recoil velocity of the excited nucleus prior to fission, and the neutron detection angle. The experimental setup which was used to detect the neutrons in coincidence with the two fission fragments is described in Sec. II. The method used for the data analysis, in particular the separation of the detected neutrons into prefission and postfission neutrons is discussed in Sec. III. The experimental results are presented in Sec. IV. They include the mass and TKE distributions of the fission fragments and the neutron multiplicities as a function of the mass and TKE of the fragments. In Sec. V the number of prefission and postfission neutrons is compared with theoretical results based on the intranuclear-cascade (INC) model and a statistical model that includes fission-evaporation competition. The experimental number of

prefission neutrons is larger than that predicted by these models. We summarize our results in Sec. VI.

II. EXPERIMENTAL ARRANGEMENT

The purpose of the experiment was the measurement of the neutrons emitted in coincidence with the two fission fragments. The 475-MeV proton beam from of the TRIUMF accelerator at the University of British Columbia was used to bombard targets of ^{209}Bi and ^{238}U. The two fission fragments were detected in position-sensitive parallel-plate avalanche counters (PPAC's). Before reaching the PPAC one of the fragment traversed a very thin multiwire proportional counter (MWPC) placed close to the target. The MWPC signal served as the start signal of a time-of-flight measurement, whereas the anode signal from the PPAC's served as the stop signals. The masses and kinetic energies were determined from the time-of-flight measurement. The neutrons were detected in two liquid scintillation detectors placed at 0° and 90° with respect to the direction of the PPAC's. A schematic view of the experimental arrangement is shown in Fig. 1.

A. The targets and scattering chamber

We used 120-μg/cm^2 ^{209}Bi targets evaporated on 40-μg/cm^2 VYNS backing and 50-μg/cm^2 ^{238}U targets on 60-μg/cm^2 VYNS backing. For the calibration we used a thin ^{252}Cf source, which was covered on both sides with 100-μg/cm^2 Ni foils and 60-μg/cm^2 VYNS foils. The Bi and U targets as well as the ^{252}Cf source were mounted on a movable target ladder in the center of the scattering chamber. The scattering chamber was made of 1.6-mm-thick aluminum and had a diameter of 62 cm. The chamber and moveable detector arms were designed to minimize neutron scattering. Special care was also taken to minimize neutron scattering and gamma background in the vicinity of the detection system. Collimation of the beam near the chamber was avoided and the beam stop was located at a distance of about 30 m from the scattering chamber.

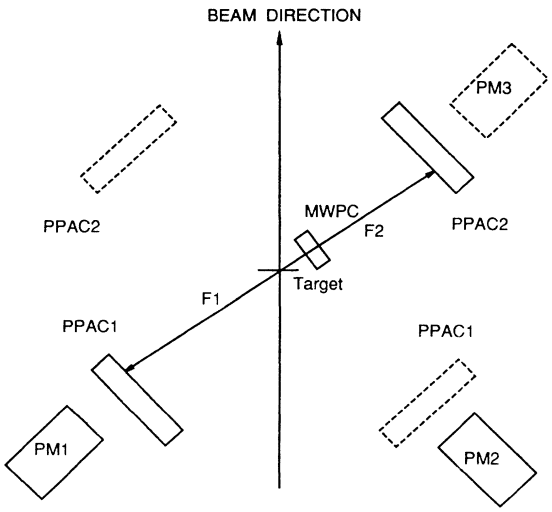

FIG. 1. Schematic view of the experimental arrangement. All fragment and neutron detectors were positioned in the reaction plane. PM3 is a *virtual* detector referred to in the data analysis (see the Appendix).

B. The fission fragments detection system

The time-of-flight of the two coincident fission fragment was measured with the aid of three low-pressure gaseous detectors. The MWPC start detector had an active area of 2×2 cm^2 and was positioned at a distance of 5.85 cm from the target center. The two cathode planes of the MWPC were made of 30-μg/cm^2 stretched polypropylene foil coated with 10-μg/cm^2 aluminum by resistive vacuum coating. The anode wire plane consisted of 10-μm-diam Au-plated tungsten wires at a 1-mm spacing. All anode wires were soldered to a common bus. The cathode-anode distance was 3.2 mm. The entrance and exit window foils of the MWPC were of 40-μg/cm^2 stretched polypropylene. Hence the total thickness of the start detector as seen by the traversing fission fragment was 160 μg/cm^2. The detector was operated at a pressure of 1.7 Torr of isobutane and at an anode voltage of 460 V. It is described in greater detail in Ref. 17.

The two stop detectors were position-sensitive parallel-plate avalanche counters very similar to that described in Ref. 18. The anode and cathode planes of the PPAC were made of 50-μg/cm^2 stretched polypropylene coated with 30-μg/cm^2 Au. On the cathode the gold coating was made in strips 5 mm wide. An intermediate wire plane, made of 100-μm-diam gold-plated tungsten wires, 2 mm apart, was mounted in the middle of the PPAC gap and was held at half the anode voltage. The wires were at 90° to the cathode strips. Both the wires and the strips were connected to tapped delay lines. The active area of the counters was 8×10 cm^2 and they were placed at a distance of 24.7 cm from the target at a polar angle of 45° and 135° with respect to the beam direction. They were operated at a pressure of 10 Torr isobutane and at an anode voltage of 730 V. Each stop detector provided five signals: the anode timing signal for the time-of-flight (TOF) measurement and two signals from each of the x and y coordinates, from both ends of the delay lines. The time difference between the two signals from each delay line provided the positions of the fragment, whereas the sum was used to eliminate double hits and events with incomplete position information. The intrinsic time resolution of the PPAC's was $\sim$250 ps [full width at half maximum (FWHM)], and the position resolution was better than 2 mm (FWHM) in the x direction and 5 mm (FWHM) in the y direction. The fragment time-of-flight system was calibrated with the aid of the thin ^{252}Cf source.

C. The neutron detectors

The neutron detectors were 12.7-cm-diam by 5.08-cm-deep cells of NE224 liquid organic scintillator. The liquid scintillator was encapsulated in an acrylic container which also served as a light guide to an RCA 4522 photomultiplier (PM) tube. The detectors were placed at a distance of 75 cm from the target, outside the scattering

chamber, at a polar angle of $\pm 135°$ with respect to the beam direction.

For the purpose of monitoring the photomultiplier gain, a green light-emitting diode (LED) was attached to the front surface of the acrylic container. The light of the LED was viewed by a solid state detector (SSD) as well as by the photomultiplier. The SSD was assumed to have a constant light detection efficiency and was used as a standard for measuring the LED light seen by the photomultiplier. The LED was periodically pulsed throughout the experiment and the photomultiplier and SSD pulses recorded on tape for off-line gain adjustment. The excellent pulse-shape discrimination characteristics of the liquid scintillator was used to discriminate between neutron and gamma interactions in the scintillator. The method used was based on the measurement of the time difference between the anode signal and the crossover time of a double-differentiated signal from the last dynode. Three signals were recorded for each neutron event: The anode signal, used for the time-of-flight measurement with respect to the start signal from the MWPC, the pulse height of the last dynode signal indicative of the energy deposited in the scintillator by the neutron or gamma ray and the pulse-shape discrimination signal.

D. Data acquisition

Events were recorded on tape sequentially. They consisted of all triple coincidences in which two fragments were detected in the fission fragment detectors and a neutron or gamma detected in one of the neutron detectors. We also recorded fission fragment events in which no neutron/gamma was detected. These events were downscaled by a factor of 8. In addition the LED pulser events were recorded. At regular intervals the data acquisition was stopped to make calibration runs with an Am-Be neutron source and with the ^{252}Cf source.

The measurements with the two targets and with the ^{252}Cf calibration source were made for two geometries. In one geometry the three fission fragment detectors were in line with neutron detector no. 1 at $+135°$ with respect to the beam direction and at 90° with respect to neutron detector no. 2. In the second geometry the fission fragment detectors were in line with neutron detector no. 2 at $-135°$ with respect to the beam and at 90° with respect to neutron detector no. 1. In this way we averaged over any systematic difference which may have existed between the two photomultipliers or positions. The start detector was always in forward hemisphere, so as to avoid scattering of neutrons emitted in the direction of the neutron detector by the material of the start detector.

III. DATA ANALYSIS

A. Measurement of the recoil momentum and mass and kinetic energy of the fission fragments

Our measurement determined the flight times of the two fission fragments between the moment the forward fragment traversed the start detector and the time the fragments were detected in the stop detectors. In order to obtain the true time of flight between target and stop detectors the measured time difference was corrected for the flight time of the forward fragment between target and start detector. The initial fragment velocities were obtained from the experimental flight times when corrected for the energy loss of the fragments in the target and detector foils. The fragment velocities together with the measured laboratory emission angles of the fragments yield the recoil velocity of the fissioning nucleus, and, assuming the mass of the fissioning nucleus is known, the two fragment masses and kinetic energies. The major uncertainty in our knowledge of the mass of the fissioning nucleus is the average number of prefission evaporation neutrons emitted from the excited nucleus. This number was measured in the present experiment. However, the average number of particles emitted in the fast (intranuclear cascade) stage of the reaction was not measured and was estimated from the intranuclear cascade calculations to be discussed below.

We show in Figs. 2 and 3 the measured recoil velocity distribution for ^{209}Bi and ^{238}U, respectively. Figures 4 and 5 show the experimental mass and kinetic energy distributions for these two targets. Figures 2–5 pertain to binary coincidence events in which no neutron was detected. We show in Table I the average value and standard deviation of the experimental recoil velocities, fragment masses, and total kinetic energies together with the predictions of the intranuclear cascade (INC) model for the recoil velocity.

B. Neutron velocity distribution and multiplicity

In order to separate neutron and gamma events a two-dimensional plot of pulse height versus pulse-shape discrimination crossover time was constructed and the best curve separating between neutron and gamma determined. Each event was checked for its position on this two-dimensional plot and accordingly logged as either a neutron or gamma event. The rejection rate of the gamma rays was about 95%, since there was of course some

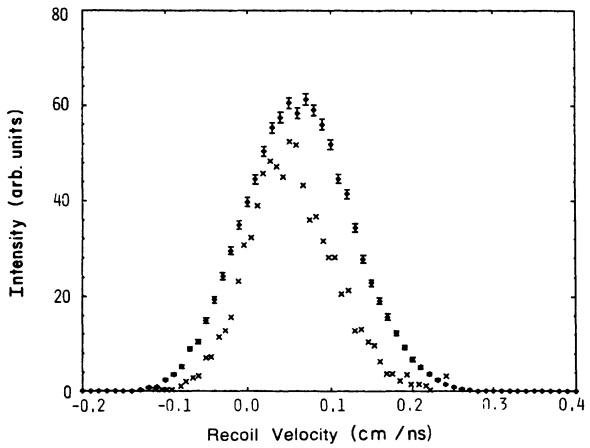

FIG. 2. The experimental recoil momentum distribution of the fissioning nucleus for the reaction of 475-MeV protons with ^{209}Bi (diamonds). Also shown is the prediction of the intranuclear cascade model (crosses).

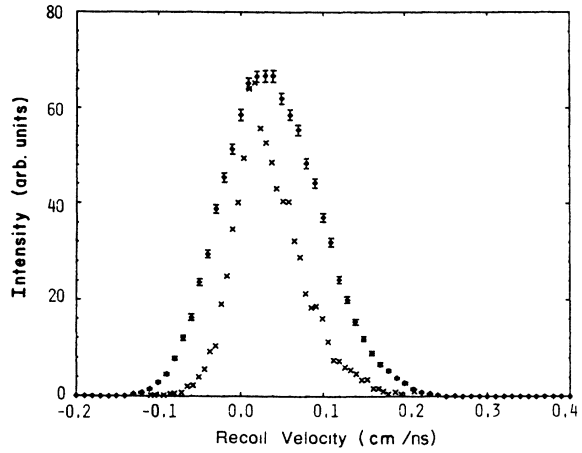

FIG. 3. Same as Fig. 2 for the reaction 475-MeV protons on ^{238}U.

overlap and we did not wish to loose too many neutron events. An Am-Be source was used to periodically check the shape and position of the (n,γ) discrimination curve.

The machine cycle of the TRIUMF accelerator is 43 ns and thus the useful period for our TOF measurement was restricted to this time interval. We also recorded the RF period preceding the true time-of-flight period and all events in this period were assumed to be random events. In our analysis they were *subtracted* from our true TOF spectrum. In this fashion we corrected to first order for random fission fragment-neutron/gamma coincidences. The random rate amounted to ~5% of the true rate for the U runs and to somewhat less for the Bi runs.

The neutron TOF was recorded with respect to the start signal of the MWPC and corrected off-line for the flight time of the fission fragment from the target to the MWPC. A software threshold at $\frac{2}{3}$ the half height of the Compton edge from a 0.511-MeV annihilation gamma ray (^{22}Na) was applied to both neutron detectors. This threshold was maintained at a constant value by correcting it for any gain shift in the photomultiplier tubes as measured by the LED-SSD combination. In practice the PM gain was very stable and a maximum variation of less that 10% was encountered when the instantaneous PM rate exceeded 20 kHz. We normally stayed well below this limit.

The neutron detection efficiency of the neutron detector was obtained from the measurement with the ^{252}Cf source. The 0° velocity distribution was compared to the results of Bowman *et al.*[19] extrapolated to 0°. The

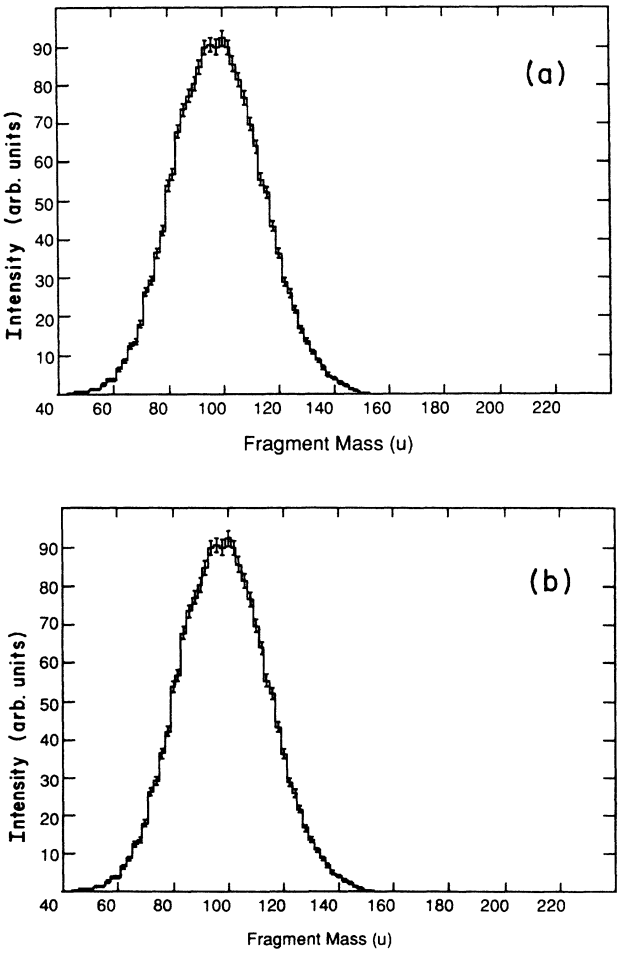

FIG. 4. The experimental fission fragment mass distributions for the fission of (a) ^{209}Bi and (b) ^{238}U.

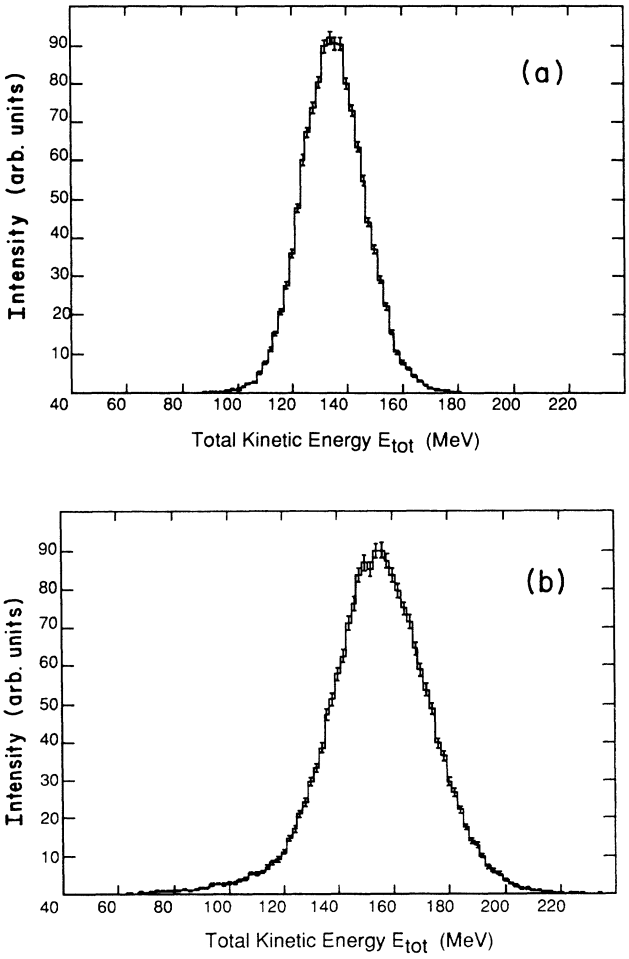

FIG. 5. The experimental total kinetic energy E_{tot} distributions of the fission fragments for (a) ^{209}Bi and (b) ^{238}U.

TABLE I. Average values and standard deviation of the recoil velocity, fragment masses, and total kinetic energies for the fission of ^{209}Bi and ^{238}U bombarded with 475-MeV protons. Also shown are the INC predictions for the recoil velocities.

Target	^{209}Bi	^{238}U
Standard deviation of mass distribution	15.8	19.4
Average total kinetic energy (MeV)	138.4	152.0
Standard deviation of total kinetic energy distribution (MeV)	10.9	19.0
Experimental average recoil velocity in beam direction (cm/ns)	0.0615	0.0380
Calculated average recoil velocity in beam direction (cm/ns)	0.0537	0.0351
Standard deviation of the experimental recoil velocity distribution in the beam direction (cm/ns)	0.0645	0.0589
Standard deviation of the calculated recoil velocity in beam direction (cm/ns)	0.0532	0.0430

overall normalization was obtained from the results of Volpi *et al.*[20] for the total number of prompt fission neutrons, $\bar{\nu}=3.725$. The efficiency of the two neutron detectors differed by $\sim 10\%$, part of which may be due to the statistical error in the ^{252}Cf calibration. Our efficiency curve (ε_n) is similar in shape to that obtained by Drosg[21] for a scintillator of NE-213 (which resembles the NE-224 used in the present experiment) of similar diameter. His efficiency curve is higher by 20% than ours, this factor being somewhat larger than expected from the difference in the depth of the scintillator used (5.7 cm for Drosg versus 5.08 cm for our scintillator).

We show in Fig. 6 typical neutron TOF spectra for the ^{209}Bi and ^{238}U targets. The time resolution (standard deviation) as obtained from the width of the gamma peak is ~ 1 ns. The TOF signals preceding the gamma peak are random coincidences. They were shifted by 43 ns and subtracted from the true TOF signal.

The neutron velocity and angular distributions were analyzed under the following two assumptions: (i) There are three sources emitting neutrons—the excited nucleus prior to fission (prefission neutrons) and the two fission fragments. (ii) The neutrons are emitted isotopically in the center-of-mass (c.m.) system of the recoiling excited nucleus prior to fission and the c.m. system of the fully accelerated fragments. In principle one has to detect the neutrons at three different laboratory angles in order to reconstruct the neutron c.m. velocity spectra of these three sources. In practice it suffices to measure the neutrons at two angles since the measurement of the neutron emission from two fragments yields identical information when accumulated over the whole fission fragment mass and energy spectrum. We therefore measured the neutron velocity spectrum at $\sim 0°$ and $\sim 90°$ with respect to the direction of the fission fragments, these two angles being the optimum choice for the separation of the neutrons into prefission and postfission neutrons.

As a first approximation we assumed that a neutron detected at 0° with respect to the fission fragment direction was emitted from that fragment and that a neutron detected at 90° with respect to the fission direction was a prefission neutron. These approximations were corrected for the contribution of prefission neutrons detected at 0° and vice versa and for the contribution of neutrons emitted from the complimentary fragment. A more detailed description of the analysis procedure is given in the Appendix. Contrary to similar procedures used in previous experiments[22] the iteration did not converge quickly. This was due to the higher excitation energies encountered in this experiment with resultant higher c.m. velocities of the postfission neutrons, which considerably reduced the focusing of the postfission neutrons in the direction of the fission fragments. One of the effects of the slow convergence of the iteration procedure was the large statistical error of the final results for the prefission and postfission neutron multiplicity, since the total in

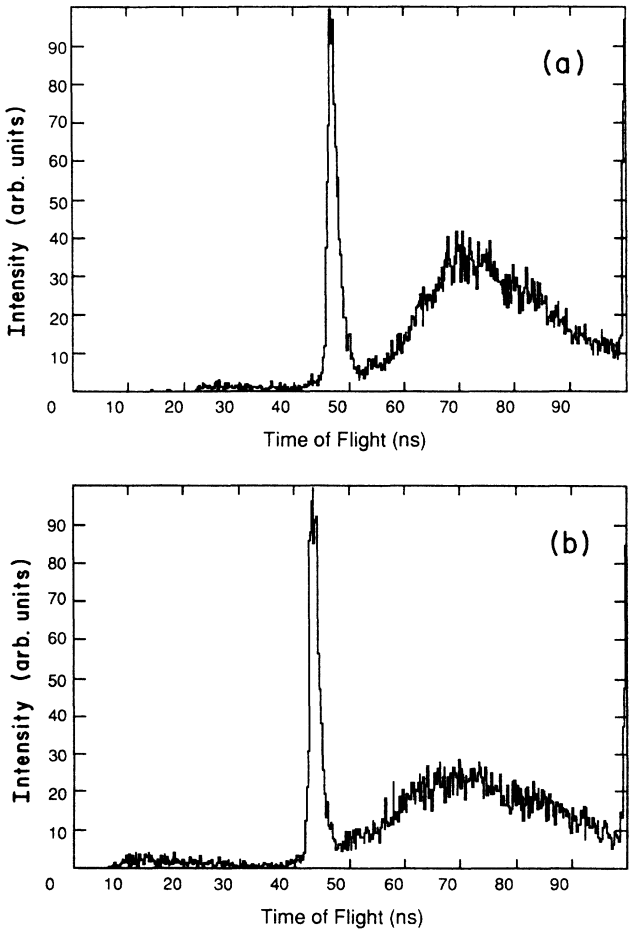

FIG. 6. Typical neutron time-of-flight spectrum for (a) ^{209}Bi and (b) ^{238}U.

each case was the sum of a considerable number of positive and negative terms of roughly equal magnitude. (The successive terms of the iteration sequence have opposite signs.) This large error affects less the experimental value of the *total* number of neutrons emitted (prefission and postfission neutrons). Another result of the ambiguity in separating prefission and postfission neutrons is a similar ambiguity in applying a recoil correction of the emitted neutrons to the fragment or prefission nucleus since the emitting source is uncertain. We therefore did not apply such a correction in our data analysis. However the results to be discussed below (including tables and figures) are independent of this assumption within the experimental accuracy.

In order to estimate the number of neutrons that were not detected because their laboratory velocity was below the experimental threshold we performed a detailed simulation calculation including all aspects of the experimental arrangement. About 20 000 simulated triple coincidence events each were created for the ^{209}Bi and ^{238}U reactions. The simulated events were analyzed in exactly the same way as the experimental results. The input parameters of the simulation were adjusted so that the mean values and standard deviations of the simulated distributions of the major experimental variables (fragment mass and total kinetic energy, recoil velocity in the beam direction and perpendicular to it, the center-of-mass velocity of the *detected* prefission and postfission neutrons) agreed with the experimental results within the experimental accuracy. (No least-squares fit was attempted because it would have required an inordinate amount of computer time.) The simulation also assured us that no systematic bias was introduced in our data analysis.

IV. EXPERIMENTAL RESULTS

We measured ~60 000 fission fragment-neutron triple coincidence events with the ^{209}Bi targets and ~120 000 such events with the ^{238}U targets. We show in Fig. 7 the laboratory neutron velocity distributions for ^{209}Bi measured at ~0° and at ~90° with respect to the direction of the fission fragment. The threshold in Fig. 7 is due to the range of the TDC's used and corresponds roughly to one machine cycle (43 ns). The two spectra are very similar in shape, indicating the large fraction of prefission neutrons, which give the same contribution to the 0° and 90° detectors. Yet the peak of the 0° distribution is at a somewhat higher value due to the effect of the postfission neutrons which have a larger contribution at 0°. The neutron velocity distributions for the ^{238}U target are very similar to the ^{209}Bi distributions.

Figure 8 shows the c.m. velocity distributions for the postfission and prefission neutrons as obtained from the iteration procedure. "Center-of-mass" refers here to the fragment c.m. for the postfission neutrons and the recoiling excited nucleus prior to fission for the prefission neutrons. We again show the ^{209}Bi results. The results for the ^{238}U target are similar in shape to the corresponding ^{209}Bi spectra. The postfission and prefission c.m. spectra do not differ substantially in their shape, and neither can be reproduced by a single Maxwellian distribution. This is not surprising in view of the expected large spread in the initial excitation energy of the fissioning nuclei. The major difference between the two spectra is the lower cutoff in the prefission spectrum due to the laboratory velocity threshold of $v_{th}=1.55$ cm/ns used in the iteration procedure. Because of the large fragment velocity this threshold essentially does not affect the postfission spectrum (see also the following). A threshold of 1.55 cm/ns was used in the analysis in order to avoid the velocity region in which the neutron detection efficiency ϵ_n increases very rapidly with velocity, causing large fluctuations in the resulting velocity spectra.

We show in Fig. 9 the total neutron distribution as a function of E_{tot}, the total kinetic energy of both fission fragments, for ^{238}U. The total number of neutrons decreases with increasing E_{tot}.

We show in Fig. 10 the number of postfission neutrons of ^{209}Bi as a function of the mass of the fragment from which they were emitted. The results for ^{238}U are similar. We see that the number of neutron increases strongly with fragment mass as it is expected if the excitation energy is equilibrated in the excited nucleus prior to

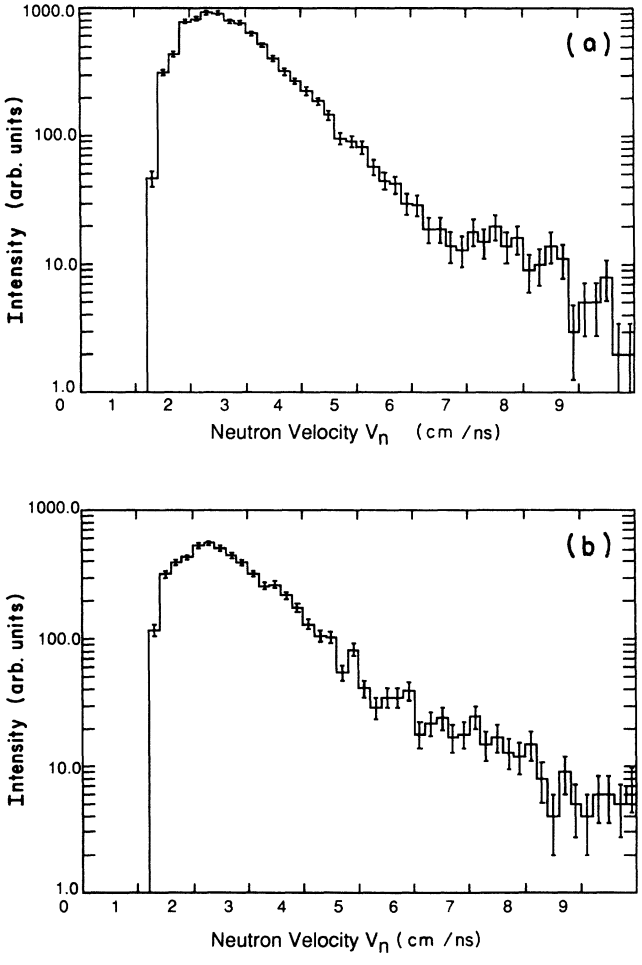

FIG. 7. Laboratory neutron velocity distribution for ^{209}Bi measured at (a) 0° and at (b) 90° with respect to the fission fragment direction.

fission. In this case the number of postfission neutrons emitted from a fragment should be roughly proportional to the fragment mass. The number of prefission neutrons, on the other hand, is independent, within statistics, of the fragment mass (Fig. 11).

Perhaps the most interesting dependence is the number of neutrons emitted as a function of the recoil velocity of the excited nucleus prior to fission since, as will be seen in the next section, the INC calculations show that there is a strong positive correlation between the size of the recoil momentum and the initial excitation energy of the nucleus at the end of the fast (INC) part of the reaction. Thus the recoil velocity of the fissioning nucleus may be assumed to be indicative of the initial excitation energy of the nucleus which later undergoes fission. We show in Fig. 12, the number of prefission neutrons as a function of the recoil velocity. Assuming the correlation between recoil velocity and initial excitation energy to hold, we find that the number of prefission neutrons rises with excitation energy.

We show in Table II the measured number of prefission and postfission neutrons, the correction factor by which the measured values have to be multiplied with and the corrected (i.e., final) values. The correction factors were obtained from the simulation calculation. They are the ratios between the input values of the calculation for the number of prefission and postfission neutrons and the values obtained when the simulated input is analyzed in exactly the same way as the experimental data. As expected, the correction factor is much larger for the prefission neutrons, since, as already mentioned, the prefission neutrons are much more affected by the lower cutoff used in the analysis than the postfission neutrons. The correlation factor for postfission neutrons is close to 1.00 (i.e., no correction needed) for both ^{209}Bi and ^{238}U. The fact that for ^{209}Bi that factor is actually somewhat smaller than one shows that in this case the analysis program "shifts" a small part of the prefission neutrons to the postfission part. (This may also be the reason that the correction factor for prefission neutrons for ^{209}Bi is somewhat larger.) The difference between the ^{209}Bi and ^{238}U factors is probably mainly due to a somewhat different shape of the prefission spectra for these two targets. Because of the relatively large errors introduced by the slow convergence of the iteration procedure we have conservatively assigned an error of 20% to the number of prefission and postfission neutrons. For the prefission

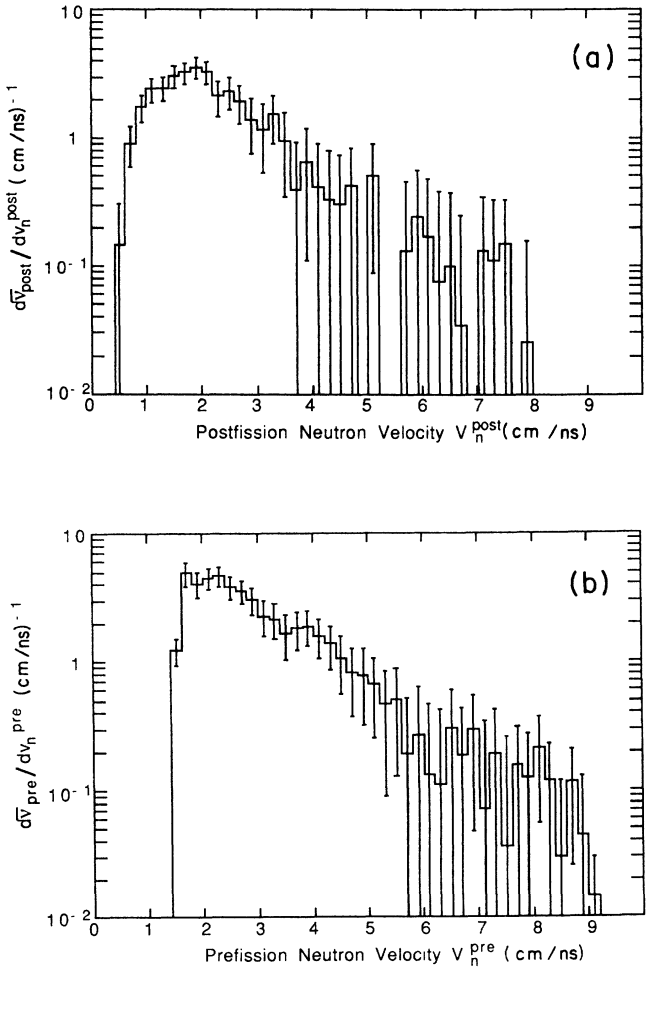

FIG. 8. Center-of-mass neutron velocity distribution $d\bar{\nu}/dv_n$ for ^{209}Bi for (a) postfission neutrons and (b) prefission neutrons.

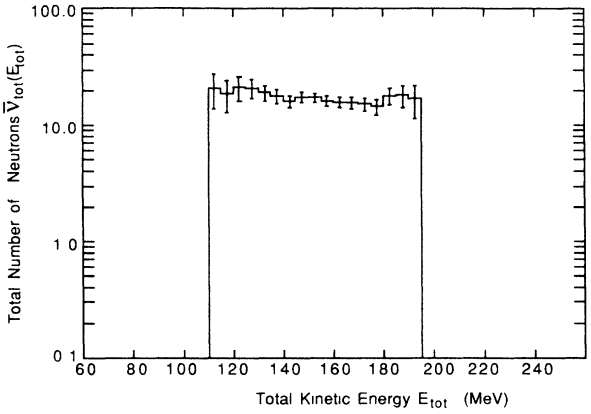

FIG. 9. The total number of neutrons emitted as a function of the total kinetic energy E_{tot} for ^{238}U.

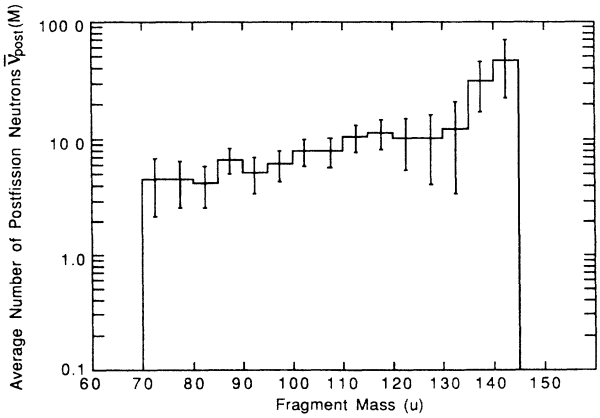

FIG. 10. The number of postfission neutrons as a function of the mass of the emitting fragment for ^{209}Bi.

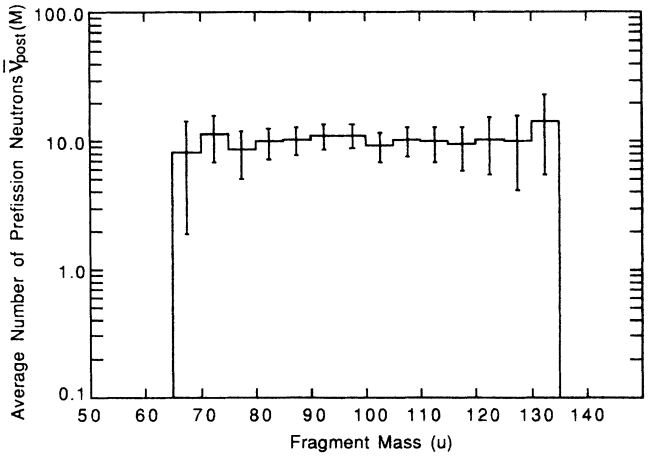

FIG. 11. The number of prefission neutrons as a function of the mass of one of the fission fragments for ^{209}Bi.

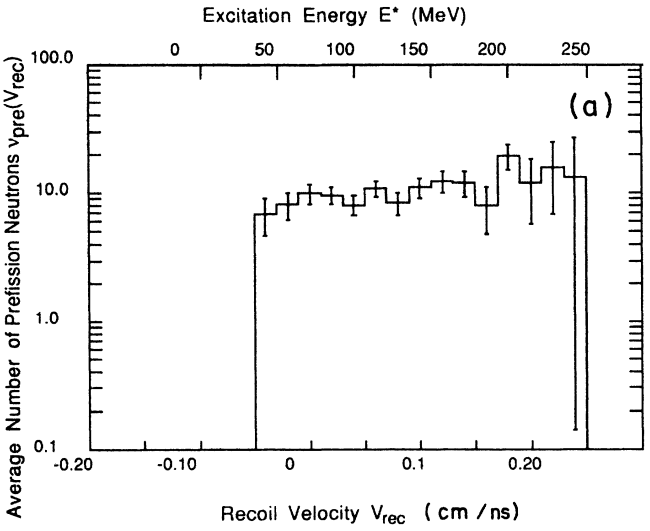

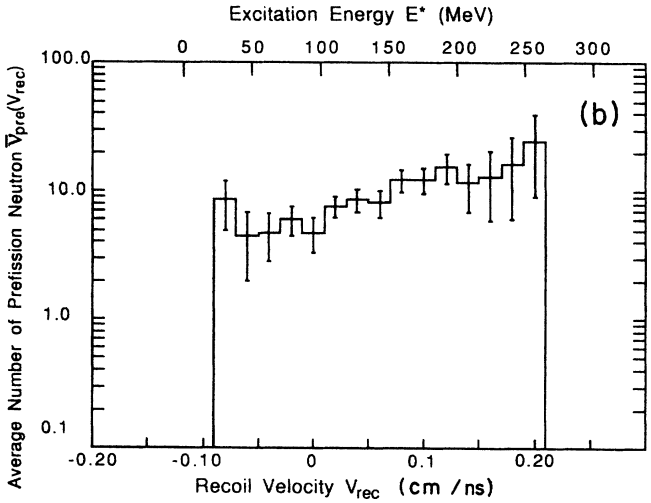

FIG. 12. The number of prefission neutrons as a function of the recoil velocity of the excited nucleus prior to fission or, alternatively, the initial excitation energy of the excited nucleus for (a) ^{209}Bi and (b) ^{238}U.

neutrons this error also takes into account the small uncertainty introduced by our lack of precise knowledge of the spectrum below the analysis threshold. Because they are less affected by the errors introduced by the iteration procedure, the error assigned to the total number of neutrons is 10%.

V. COMPARISON WITH THE PREDICTION OF THEORETICAL MODELS

We have calculated the number of prefission neutrons assuming that the reactions 475-MeV $p+^{209}$Bi, ^{238}U proceed in the two steps: (1) a fast step in which the incoming proton makes a series of collisions with the individual nucleons of the target nucleus and thus gives rise to an intranuclear cascade in which a number of fast nucleons are emitted and the residual nucleus is left in a highly excited state and (2) the excited nucleus deexcites through statistical emission of particles (mostly neutrons for the heavy targets considered here) or fissions. It is this competition between statistical particle emission and fission that is our main interest in the present work. However, the first, fast, step of the reaction must be calculated in order to obtain the distribution in A,Z excitation energy and angular momentum of the excited nuclei, which are the starting conditions for the second, slow, step of the reaction.

We calculated the intranuclear cascade (INC) step of the reaction using the INC simulation code ISABEL.[23] Though primarily used in the past to calculate high-energy nucleus-nucleus reactions, this code may be used equally well to calculate high-energy proton-nucleus reac-

TABLE II. The prefission and postfission neutron multiplicity as well as the total number of neutrons emitted in the fission of ^{209}Bi and ^{238}U bombarded with 475-MeV protons.

Target		^{209}Bi	^{238}U
Average number of prefission neutrons (measured)	$\bar{\nu}_{pre}^{expt}$	6.19	5.92
Correction factor for prefission neutrons	F_{pre}	1.60	1.42
Corrected number of prefission neutrons	$\bar{\nu}_{pre}^{corr}$	9.90±1.98	8.40±1.68
Average number of postfission neutrons (measured)	$\bar{\nu}_{post}^{expt}$	7.47	8.01
Correction factor for postfission neutrons	F_{post}	0.96	1.08
Corrected number of postfission neutrons	$\bar{\nu}_{post}^{corr}$	7.20±1.44	8.56±1.67
Total number of neutrons emitted	$\bar{\nu}_{tot}$	17.10±1.71	17.05±1.71
Theoretical number of prefission neutrons		6.05	3.90

tions. The recoil velocity distribution of the excited nucleus at the end of the fast (INC) part of the reaction as predicted by the ISABEL code is shown in Fig. 2 for ^{209}Bi and in Fig. 3 for ^{238}U together with the experimental distributions. The agreement between the calculated and experimental results is surprisingly good in view of the fact that there are essentially no free parameters in the calculation. The good agreement between the INC model (ISABEL) and the experimental recoil distribution gives us confidence in the other predictions of the model. We show in Fig. 13 the average mass M, the average excitation energy E^*, and the average angular momentum I of the excited nucleus at the end of the fast cascade as a function of the recoil velocity. Also shown is the average impact parameter b of the incoming proton at the beginning of the reaction as a function of the recoil velocity of the excited nucleus. The error bars indicate the standard deviation of these distributions for a given recoil velocity. We see that the mass M and impact parameter b have their maximum at $V_{\text{rec}}=0$ and decrease as the absolute value of the recoil velocity increases and the reverse is true for the excitation energy E^* and angular momentum I of the excited nucleus. Figure 14 shows a contour plot of the excitation energy and angular momentum distribution predicted by the INC model for 475-MeV protons on ^{209}Bi. These distributions together with the mass and charge distributions as predicted by the INC model, serve as the input for the calculation of the second stage of the reaction in which particle evaporation competes with fission.

The deexcitation of the excited nucleus by particle evaporation and fission was calculated with the statistical model code PACE-2.[24] The program calculates neutron, proton, and alpha-particle evaporation using the Hauser-Feshbach formalism, γ-ray emission, and fission. We used the angular-momentum-dependent fission barriers as calculated by Sierk[25] for the calculation of the fission width. The calculation of the barriers takes into account the effect of the diffuse surface of the nucleus. For the level densities we used the expression of Gilbert and Cameron[26] with the level density parameter of $a=A/8$. The Bohr-Wheeler[1] expression was used to calculate the fission width. This calculation does not take into account the corrections due to the shell effects in the ground states of nuclei close to the ^{208}Pb doubly closed shell and the double-humped barrier in the actinides region. It also ignores the contribution of the neutrons of the fast stage of the reaction to the measured neutrons. However, the ISABEL calculations show that in the angular range of 125°–145° and laboratory energy range below 10 MeV this contribution is less than 2% of the experimentally observed yield.

The most important prediction of the ISABEL–PACE-2 calculation in our context is the number of neutrons evaporated prior to fission. These values for ^{209}Bi and ^{238}U are given in Table II together with the experimental results. We see that the calculated values are substantially smaller than the experimental ones for both targets.

VI. CONCLUSIONS

The main results of the present investigation are summarized in Table II.

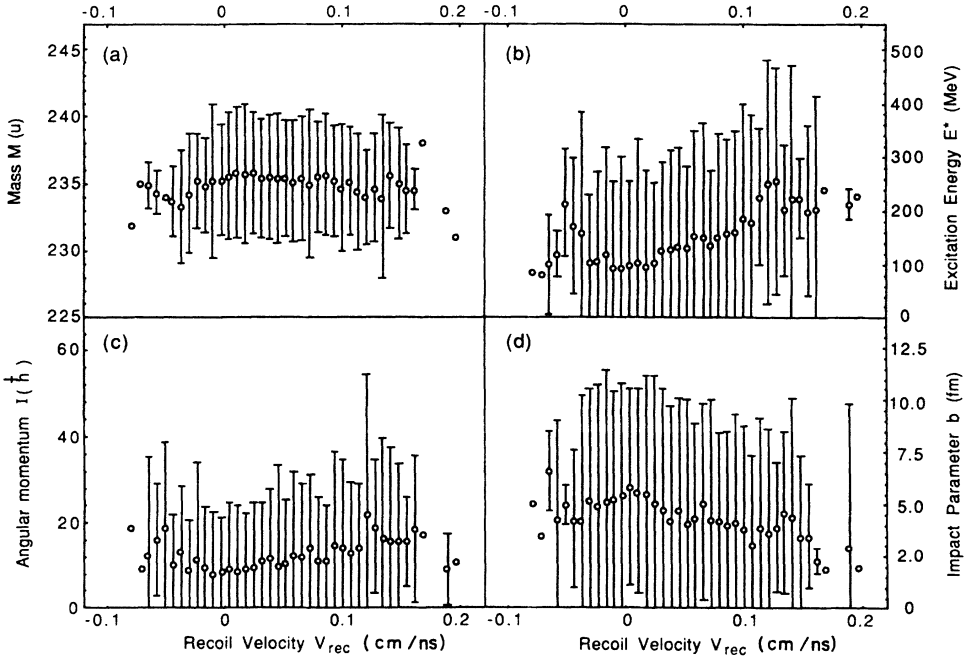

FIG. 13. The prediction of the INC model for (a) the average mass M, (b) average excitation energy E^*, and (c) average angular momentum I of the excited nucleus at the end of the fast intranuclear cascade stage of the reaction as a function of the recoil velocity of the nucleus for 475-MeV protons on ^{238}U. Also shown is (d) the average impact parameter b of the incoming proton. The error bars give the standard deviation of the distributions of the variables.

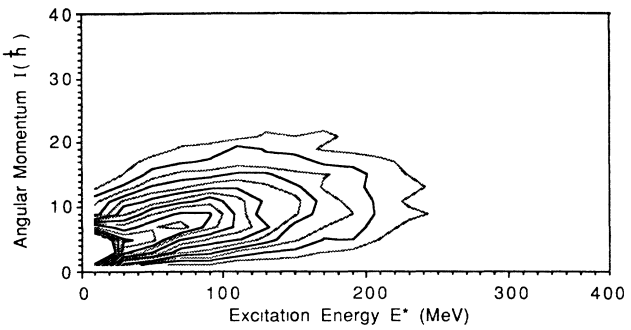

FIG. 14. Contour plot of the excitation energy vs angular-momentum distributions as predicted by the intranuclear cascade model for 475-MeV protons on ^{238}U.

(1) The total number of neutrons emitted in the fission of ^{209}Bi and ^{238}U when bombarded by 475-MeV protons is ~ 17 for both targets within an error of 10%.

(2) The number of prefission neutrons and postfission neutrons is similar, i.e., fission occurs on the average approximately halfway through the statistical deexcitation process.

(3) Calculations based on the statistical model using the Bohr-Wheeler formula for the fission width and the Sierk formulation for the angular-momentum-dependent fission barriers substantially underestimate the number of prefission neutrons for both targets, but they also predict a larger number of prefission neutrons for ^{209}Bi. Except for the absolute numbers our results qualitatively are very similar to the results obtained by Cheifetz *et al.*[27] for a similar experiment done with 150-MeV protons.

The conclusion that the statistical model calculations overestimate the fission probability at high excitation energy, and thus underestimate the number of neutrons emitted prior to fission, is not surprising in view of the fact that the Bohr-Wheeler formula ignores the effect of dissipation on the fission width at high excitation energies as was pointed out in the introduction. Our results give further credence to the view that the reduction in the fission probability is indeed due to its hindrance at high excitation energies and not due to any effect associated with high angular momenta (which in general would increase the fission width rather than decrease it), since proton-induced reactions do not produce high angular momenta.

Finally, the number of postfission neutrons emitted from a given fragment increases with the mass of that fragment (Fig. 12). Such a relationship is expected if the excitation energy of the fissioning nucleus is equilibrated and the initial "temperature" of the two fragments is the same. Not surprisingly, the number of prefission neutrons is independent of the fragment mass (Fig. 11).

ACKNOWLEDGMENTS

A.B. and Z.F. would like to thank Dr. Erich Vogt, the Director of the TRIUMF Laboratory, for the hospitality accorded to them during the preparation of the experiment and the actual data taking and analysis. They also gratefully acknowledge the financial support of the Gordon M. Shrum Fund and a Hettie H. Hamman Research Fellowship. This work was partially supported by the National Research Council of Canada and the Natural Sciences and Engineering Research Council of Canada.

APPENDIX: THE EVENT-BY-EVENT ANALYSIS

In this appendix we describe in some detail the procedure used in the event-by-event analysis of the neutron-fission fragment coincidence data. As explained in Sec. III the analysis is based on the assumption that all neutrons originate from one of two sources: (1) the recoiling excited nucleus after the end of the intranuclear cascade, and before fission; or (2) the two fully accelerated fission fragments after fission occurred. The neutrons are assumed to be emitted isotropically in the c.m. frame of these sources. The c.m. spectra of the neutrons are calculated from the measured neutron spectra in the two scintillation detectors located at 0° and 90° with respect to the backward directed fission fragment, at an angle of $\theta = \pm 135°$ with respect to the beam direction. Our calculation is based only on the "high velocity" neutrons, i.e., those which are emitted in the respective c.m. system in the direction of the neutron counters. Thus when a neutron is detected in the neutron detector in the direction of the backward fission fragment detector (PM1 in Fig. 1) it is accepted for analysis if

$$v_n \geq V_F \cos\theta_n \ , \tag{1}$$

where v_n is the laboratory velocity of the neutron, V_F is the laboratory velocity of the fragment $F1$ detected in PPAC1, and θ_n is the laboratory angle between the fission fragment and the neutron. For a neutron detected in PM2, at 90° with respect to the fission fragment direction the condition is

$$v_n \geq V_{\rm rec} \cos\theta_n \ , \tag{2}$$

where $V_{\rm rec}$ is the recoil velocity of the prefission nucleus [compound nucleus (CN)] (assumed to be collinear with the beam direction) and θ_n is the angle between the recoil direction and the 90° neutron counter. [Note that normally the recoil is in the beam direction and condition (2) is then always satisfied, but even in the rare cases when the recoil momentum is in the backward direction, condition (2) is almost always true due to the small value of the recoil velocity.]

Let us now follow the iteration procedure used if a neutron is detected in the 0° neutron counter (PM1). We assume that it was emitted from the fission fragment $F1$ detected in the direction of the neutron counter PM1, i.e., we *assume* it is a *postfission* neutron. If condition (1) is satisfied we find the neutron velocity in the fission fragment $F1$ c.m. system

$$v_{\rm c.m.} = (v_n^2 + V_{F1}^2 - 2 v_n V_{F1} \cos\theta_n)^{1/2} \ , \tag{3}$$

and the event is added to the array $N_{\rm post}(v_n, M_1, E_{\rm tot}, V_{\rm rec})$, where M_1 is the mass of the fission fragment $F1$, $E_{\rm tot}$ the total kinetic energy of both fragments and $V_{\rm rec}$ is the recoil velocity of the nucleus

prior to fission. The weight $W_{\text{c.m.}}$ which is given to this event in array N_{post} is determined by the Jacobian of the transformation, the detection efficiency ϵ_n and the solid angle $\Delta\Omega_n$

$$W_{\text{c.m.}} = \frac{v_{\text{c.m.}}(V_n - V_{F1}\cos\theta_n)}{v_n^2} \frac{4\pi}{\epsilon_n \Delta\Omega_n} . \tag{4}$$

Next we calculate whether a neutron with velocity $v_{\text{c.m.}}$ emitted from fragment $F1$ could have reached the *hypothetical* neutron detector PM3 in the direction of the *complementary* fission fragment $F2$ and would have been identified as having been emitted from $F2$.

We check whether

$$v_{\text{c.m.}} \geq V_{F1}\sin\theta_K ,$$

where θ_K is the angle between fragment $F1$ and PM3. The laboratory velocity of the neutron in the detector PM3 is

$$v_K = V_{F1}\cos\theta_K \pm (v_{\text{c.m.}}^2 - V_{F1}^2 \sin^2\theta_K)^{1/2} . \tag{5}$$

[We can neglect the negative solution of Eq. (5), since θ_K is always close to 180° and hence $\cos\theta_K < 0$.] If there exists a positive solution for v_K, a neutron with c.m. velocity $v_{\text{c.m.}}$ emitted from $F1$ can reach PM3 and would have been (erroneously) recorded as being emitted from fragment $F2$.

The initial weight of this event is

$$W_K = \frac{v_n - V_{F1}\cos\theta_n}{v_K - V_{F1}\cos\theta_K} \frac{v_K^2}{v_n^2} \frac{\epsilon_K}{\epsilon_n} , \tag{6}$$

where ϵ_n is the detection efficiency of a neutron of velocity v_n in PM1 and ϵ_K the corresponding efficiency of a neutron of velocity v_K in PM3. (ϵ_n^{-1} signifies the fact that the number of neutrons of velocity $v_{\text{c.m.}}$ *emitted* by fragment $F1$ is ϵ_n^{-1} times the number actually *detected* by PM1, and ϵ_K signifies the probability that a neutron of velocity v_K is detected by PM3.)

Finally we have to project the event into the c.m. system of $F2$ if

$$v_K \geq V_{F2}\cos\theta_L \tag{7}$$

where θ_L is the angle between the direction of $F2$ and PM3. We find

$$v'_{\text{c.m.}} = (v_K^2 + V_{F2}^2 - 2v_K V_{F2}\cos\theta_L)^{1/2}$$

and the final weight given to this event in $N_{\text{post}}(v'_{\text{c.m.}}, M2, E_{\text{tot}}, V_{\text{rec}})$ is

$$W_L = -W_K \frac{v'_{\text{c.m.}}(v_K - V_{F2}\cos\theta_L)}{v_K^2} \frac{1}{\epsilon_K} . \tag{8}$$

The negative sign is due to the fact that the neutron was actually emitted by $F1$, and hence its contribution to the neutrons emitted by $F2$ is negative. (We see that the final weight W_L is independent of ϵ_K, as it should be, since the "true" number of neutrons is equal to ϵ_n^{-1} and independent of ϵ_K.)

Next the same procedure is repeated with respect to the possibility of the neutron of c.m. velocity $v_{\text{c.m.}}$ emitted from $F1$ reaching PM2 and being (erroneously) assumed to be emitted from the "compound" nucleus CN recoiling with recoil velocity V_{rec}. We first check whether

$$v_{\text{c.m.}} \geq v_{F1}\sin\theta_M ,$$

where θ_M is the angle between fragment $F1$ and the neutron detector PM2. The laboratory velocity of the neutron in the direction of PM2 is

$$v_M = V_{F1}\cos\theta_M \pm (v_{\text{c.m.}}^2 - V_{F1}^2 \sin^2\theta_M)^{1/2} . \tag{9}$$

Next we check whether

$$v_M \geq V_{\text{rec}}\cos\theta_R , \tag{10}$$

where θ_R is the angle between the recoil direction and PM2 (θ_R normally differs from 135° since the direction of V_{rec} is not necessarily in the horizontal plane). Finally, the weight given to the event in the array $N_{\text{pre}}(v''_{\text{c.m.}}, M_1, E_{\text{tot}}, V_{\text{rec}})$

$$W_M = -\frac{(v_n - V_{F1}\cos\theta_n)}{(v_M - V_{F1}\cos\theta_M)} \frac{v''_{\text{c.m.}}(v_M - V_{\text{rec}}\cos\theta_R)}{v_n^2} \frac{1}{\epsilon_n} , \tag{11}$$

where $v''_{\text{c.m.}}$ is the neutron velocity in the c.m. system of CN, the recoiling nucleus prior to fission

$$v''_{\text{c.m.}} = (v_M^2 + V_{\text{rec}}^2 - 2v_M V_{\text{rec}}\cos\theta_R)^{1/2} . \tag{12}$$

[Again we normally can neglect the negative solution of Eq. (9), since in this case $\theta_M \simeq \pi/2$ and hence the first terms on the right-hand side of Eq. (9) is very small.]

The second iteration starts with a neutron of laboratory energy v_K emitted from $F2$ with a weight W_L. We calculate its contribution to $F1$ and CN.

Similarly for the contribution from the *first* iteration to CN. Depending on the value of v_n and V_{F1} up to five such iterations, are performed. For most detected neutrons the procedure converges after fewer iterations, i.e., the contribution of the higher iterations are negligible or zero.

The procedure is very similar if the neutron is detected in PM2. We then assume as a first approximation that it was emitted from CN prior to fission, i.e., it is a prefission neutron. We calculate its contribution to the arrays N_{pre} and N_{post} in a similar fashion as described earlier with the roles of $F1$ and CN and of PM1 and PM2 interchanged.

[1]N. Bohr and J. A. Wheeler, Phys. Rev. **56**, 426 (1939).
[2]H. A. Kramers, Physica **7**, 284 (1940).
[3]P. Grangé and H. A. Weidenmüller, Phys. Lett. **96B**, 26 (1980).
[4]P. Grangé, S. Hassani, H. A. Weidenmüller, A. Gavron, J. R. Nix, and A. J. Sierk, Phys. Rev. C **34**, 209 (1986).
[5]H. Hofmann and J. R. Nix, Phys. Lett. **122B**, 117 (1983).
[6]S. Hassani and P. Grangé, Phys. Lett. **137B**, 281 (1984); Z. Phys. A **325**, 95 (1986).
[7]A. Gavron *et al.*, Phys. Lett. B **176**, 312 (1986); A. Gavron *et al.*, Phys. Rev. C **35**, 579 (1987).
[8]A. Gavron *et al.*, Phys. Rev. Lett. **47**, 1255 (1981); **48**, 835(E) (1982).
[9]E. Holub, D. Hilscher, G. Ingold, U. Jahnke, H. Orf, and H. Rossner, Phys. Rev. C **38**, 252 (1983).
[10]D. Ward, R. J. Charity, D. J. Hinde, Jr., R. Leigh, and J. O. Newton, Nucl. Phys. **A403**, 189 (1983).
[11]D. J. Hinde, R. J. Charity, G. S. Foote, J. R. Leigh, J. O. Newton, S. Ogaza, and A. Chatterjee, Phys. Rev. Lett. **52**, 986 (1984).
[12]W. P. Zank, D. Hilscher, G. Ingold, U. Jahnke, M. Lehmann, and H. Rossner, Phys. Rev. C **33**, 519 (1986).
[13]D. J. Hinde, R. J. Charity, G. S. Foote, J. R. Leigh, J. O. Newton, S. Ogaza, and A. Chatterjee, Nucl. Phys. **A452**, 550 (1986).
[14]D. J. Hinde, J. R. Leigh, J. J. M. Bokhorst, J. O. Newton, R. L. Walsh, and J. W. Boldeman, Nucl. Phys. **A472**, 318 (1987).
[15]J. O. Newton, D. J. Hinde, R. J. Charity, J. R. Leigh, J. J. M. Bokhorst, A. Chatterjee, G. S. Foote, and S. Ogaza, Nucl. Phys. **A483**, 126 (1988).
[16]D. J. Hinde, H. Ogata, M. Tanaka, T. Shimoda, N. Takahashi, A. Shinohara, S. Wakamatsu, K. Katori, and H. Okamura, Phys. Rev. C **37**, 2933 (1988).
[17]A. Breskin, Nucl. Instrum. Methods **196**, 11 (1982).
[18]Y. Eyal and H. Stelzer, Nucl. Instrum. Methods **155**, 157 (1978).
[19]H. R. Bowman, S. G. Thompson, J. C. D. Milton, and W. J. Swiatecki, Phys. Rev. **126**, 212D (1962).
[20]A. Volpi and K. G. Progress, Phys. Rev. C **1**, 683 (1970).
[21]M. Drosg, Nucl. Instrum. Methods **105**, 573 (1972).
[22]I. Tserruya *et al.*, Phys. Rev. C **26**, 2509 (1982).
[23]Y. Yariv and Z. Fraenkel, Phys. Rev. C **20**, 2227 (1979); **24**, 488 (1981).
[24]A. Gavron, Phys. Rev. C **21**, 230 (1980).
[25]A. J. Sierk, Phys. Rev. C **23**, 2039 (1986).
[26]A. Gilbert and A. G. W. Cameron, Can. J. Phys. **43**, 1446 (1965).
[27]E. Cheifetz, Z. Fraenkel, J. Galin, M. Lefort, J. Péter, and X. Tarrago, Phys. Rev. C **2**, 256 (1970).